Climate Change Initiative
Living Planet Fellowship

2014

Simon Munier

Estellus

400112805/15/I-SBo

European Space Agency
Agence spatiale européenne

STANDARD COVER PAGE FOR ESA STUDY CONTRACT REPORTS

ESA STUDY CONTRACT REPORT		
ESA Contract No: **400112805/15/I-SBo**	**Subject:** **Surface water and climate variability from a high-resolution GIEMS-SAR merged product**	**Contractor:** **Estellus**
ESA CR( ) No.	**No. of Volumes: 1** **This is Volume No.: 1**	**Contractor Reference:**

Abstract:

Terrestrial surface water, identified as an Essential Climate Variable by the Global Climate Observing System, is a key parameter of the global water and biogeochemical cycles and plays an important role in the climate system and its variability. However, the knowledge of the global distribution and dynamics of surface water remains limited. A Global Inundation Extent from Multi-Satellite (GIEMS) dataset of monthly inundation and surface water dynamics at about 25 x 25 km2 resolution has been produced by a multi-sensor analysis covering 1993-2007. In spite of the high value of this dataset for hydrology and climate studies, its low-resolution limits the observations to only 20% of the global inland surface water, whereas it would be 80% with a 100 x 100 m2 resolution. In this project the GIEMS product and SAR data from the Sentinel-1 mission are merged in order to produce a dataset of high resolution monthly maps of surface water extent. Sentinel-1 SAR data were processed and used to set up a downscaling method that was applied on the GIEMS product over the whole time period (back to 1993 and up to present). Two methodologies are proposed that rely on the construction of a "floodability" index defined for each high-resolution pixel as the probability of being inundated. The first method uses different topographic indicators (such as elevation, slopes, distances to the main rivers) derived from HydroSHEDS elevation database, and has the advantage of being extendable to the global scale. The second method, which is shown to be more accurate, is based on SAR data but requires several images of the same region at different hydrological states. Both methods were applied on a region of the Danube Basin and the resulting downscaled water maps were analyzed and compared. In a future work, the value of the merged product for hydrology and climate purposes will be assessed by statistical and frequential analyses, at local to regional scale, of the temporal and spatial characteristics of the surface water extent and comparisons with climate and anthropogenic indicators will be performed. The GIEMS-SAR product will then possibly help climate change mitigation related to water surfaces.

The work described in this report was done under ESA Contract. Responsibility for the contents resides in the author or organisation that prepared it.

Names of Authors:
Simon Munier, Filipe Aires and Catherine Prigent (Estellus, Paris, France)

NAME OF ESA STUDY MANAGER	ESA BUDGET HEADING
Stephen Plummer **DIV: EOP-SC** **DIRECTORATE: EOP**	

Surface water and climate variability from a high-resolution GIEMS-SAR merged product

1 Introduction

Terrestrial surface water, identified as an Essential Climate Variable by the Global Climate Observing System, is a key parameter of the global water and biogeochemical cycles and plays an important role in the climate system and its variability. Changes in global surface water extent are closely related to changes in the global carbon cycle (CO2 and methane emission). Meanwhile, the global average maximum inundated area has significantly declined over the last decades, partly due to population pressure (Prigent et al., 2012). However, the knowledge of the global distribution and dynamics of surface water remains limited. Despite the advent of satellite remote sensing techniques for hydrologic investigations over the last 20 years, frequent accurate high-resolution characterization of the temporal and spatial variation of surface water is beyond the capabilities of current satellite methods. Therefore, important science questions remain currently unanswered. For instance, the part of the total interseasonal and interannual variation in terrestrial water storage that is attributable to lakes is still unknown.

A Global Inundation Extent from Multi-Satellite (GIEMS) dataset of monthly inundation and surface water dynamics at about 25 x 25 km^2 resolution has been produced by a multi-sensor analysis covering 1993-2007 (Prigent et al. 2001). In spite of the high value of this dataset for hydrology and climate studies (Prigent et al. 2001, 2007, 2012; Papa et al. 2010), its low-resolution limits the observations to only 20% of the global inland surface water (small water bodies are not detected), whereas it would be 80% with a 100 x 100 m^2 resolution (Downing et al., 2006).

Despite their lack of temporal coverage, many studies (e.g., Lewis and Henderson, 1998) have successfully used Synthetic Aperture Radars (SAR) to map inundation and wetland vegetation with high spatial resolution (Rosenqvist et al. 2000). One comprehensive study of flooding in the Amazon basin for low-water (September-October 1995) and high-water (May-June 1996) conditions is that of Hess et al. (2003), where wetland extent was mapped for the central Amazon region using L-band SAR imagery acquired by the Japanese Earth Resources Satellite 1 (JERS-1). For a large wetland area of the central Amazon region, dual-season radar mosaics were used to map inundation extent and vegetation at about 90 m resolution. As described in detail in Hess et al. (2003), polygon-based segmentation and clustering were used to delineate wetland extent with an accuracy of 95% along with a pixel-based classifier to map wetland vegetation and flooding state based on backscattering coefficients of two-season class combinations, producing the first high-resolution wetlands map for the region. Similarly, Kuenzer et al. (2013a,b) extracted high-resolution (150 m) inundation maps over the Mekong Delta using ENVISAT ASAR Wide Swath Mode data sets between 2007 and 2011. Since the end of 2014, the ESA Sentinel-1 satellites produces C-band SAR data with a spatial resolution of 5x20 m in Interferometric Wide Swath mode. One major drawback of mapping high-

resolution inundation maps from SAR data sets is their temporal coverage (for instance, ENVISAT ASAR data are available since 2002 only), which highly limits hydrological studies that requires long time series, especially in the context of climate change (e.g. trends or interannual variability analyses).

At the time of the proposal writing, we expected to have enough Sentinel-1 SAR retrievals, but despite our inquiries, this type of dataset (enough temporal and spatial coverage) is not yet available. We therefore had to develop our own Sentinel-1 SAR retrieval (with the collaboration of Binh Pham at the Paris Observatory), which was not the topic of this study. However, we think that this additional work was positive for the overall study.

The main question of this project is: would it be possible to develop a SAR-based downscaling methodology to derive high-resolution surface water extent from the existing GIEMS low-resolution dataset? Since GIEMS has a global coverage, the ideal situation would be to develop a downscaling technique general enough to work in all environments. However, each hydrological basin has its own characteristics, such as its topography or space-time variability. The downscaling algorithm might need to take into account these specificities and the availability of the a priori high spatial resolution information for a particular basin. About 15 years of IR/VIS images from are now available at the global scale and may be used as a reference to downscale the GIEMS product (Aires et al., 2014), but the spatial resolution is much lower than with SAR data (250m vs 20m) and images are limited by cloud cover. This of course limits the use of this type of data to clear sky scenes (in addition to low vegetation). High-resolution datasets based on topography are another option to serve as a basis for the GIEMS downscaling. Even though this method can provide good results (Fluet-Chouinard et al., 2015), it may not well capture inundations in flat regions or regions affected by man. SAR experiment over Amazon was also tested (Aires et al., 2013) but this study was limited to the use of the two available states of inundation for Amazon (low and high inundation state). With the Sentinel-1 SAR data, new approaches can be developed due to their temporal and spatial coverage. The present project aims at developing methodologies to merge in an optimal way the GIEMS product with SAR data sets in preparation for the Sentinel-1 SAR data exploitation.

2 Main objectives and study case

In this project, it is proposed to merge the GIEMS product and SAR data in order to produce a global dataset of monthly maps of surface water extent at the SAR spatial resolution. The methodology would make it possible to produce high spatial resolution inundation maps, for the full GIEMS time period (back to 1993 and up to present). In future work, the value of the merged product for hydrology and climate purposes could be assessed by statistical and frequential analyses, at local to regional scale. The temporal and spatial characteristics of the surface water extent could be compared to climate and anthropogenic indicators. The GIEMS-SAR product could then possibly help climate change mitigation related to water surfaces.

At this time, due to bandwidth data transmission limitations, the spatial coverage of Sentinel-1 SAR observations has been limited to a few regions around the world. In particular, the Europe region has been the primary focus and a large amount of observations are now available over this region. It is also a densely populated region where inundations have a high financial cost. For these reasons, the methodology developed in this study was applied and tested over a part of the Danube Basin, namely the area surrounding Bratislava and Budapest (Fig. 1). This region is of primary importance in hydrology because of frequent floods, as for example in 2013 when a major flood caused very large material and human damages.

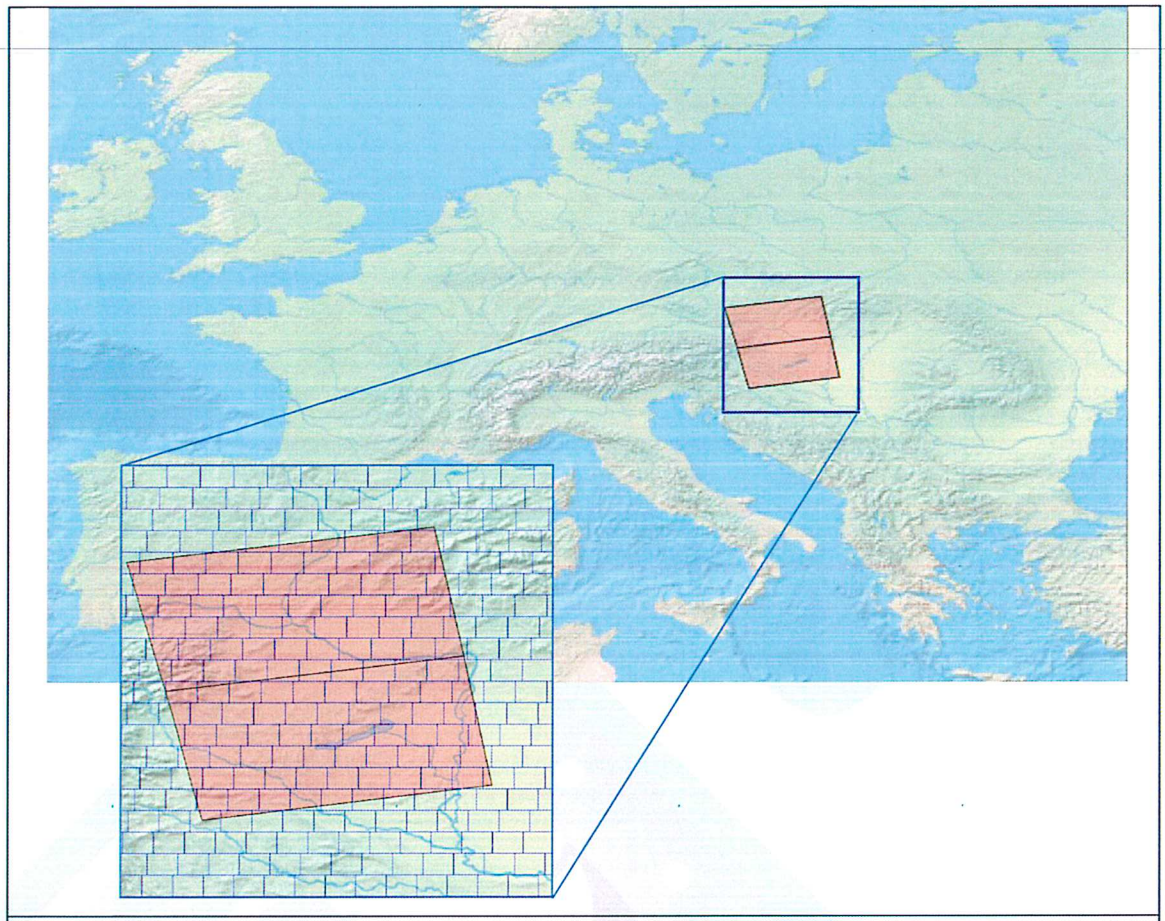

Fig. 1. Region of interest in this study. The two red patches represent the surface extent of Sentinel-1 observations (relative orbit 73, slice 11 and 12). The blue rectangle represents the 5°x5° HydroSHEDS tile. The 0.25°x0.25° grid of the GIEMS product is represented in blue in the zoom inset.

3 Overall methodology

High resolution inundation maps, derived from Sentinel-1 SAR observations, have been processed and used to set up a downscaling method that has been applied on the GIEMS product over the whole time period. Two methodologies are proposed that rely on the construction of a "floodability" index defined for each high-resolution pixel as the probability of being inundated. The first method uses different topographic indicators (such as elevation, slopes, distances to the main rivers), and has the advantage of being easily extendable to the global scale. The second method, which is expected to be more accurate, only uses high resolution inundation maps but requires several images of the same region at different hydrological states. Both methods have been tested over a small region of the Danube Basin (Fig. 1). The topography-based method has been extended to the global scale.

3.1 Downscaling principle

The main objective of the project is to provide methodologies to downscale the GIEMS product (about 25x25 km2 resolution). The GIEMS product consists in monthly inundation maps over the 1993-2007 period - an extension to the recent period is under investigation. More precisely, for each month and each low resolution pixel, GIEMS gives the fraction of the pixel area that is flooded. The

basic idea of the downscaling procedure consists in distributing the flooded area inside the low resolution (LR) pixel among high resolution (HR) pixels. To do so, a floodability index is first derived, which represents the probability of each HR pixel to be inundated. The floodability index is essentially used to create a hierarchy among the HR pixels for the allocation of the GIEMS flooded area. For instance, if a LR pixel is 30 % inundated, the first 30 % of the HR pixels (according to the floodability index) will be inundated. Assuming that the floodability is constant in time (i.e. no major changes in the floodplain geomorphology), the floodability index can be used over the whole GIEMS period (1993-2007), even though it is based on more recent observations (such as Sentinel-1 SAR data).

Two main products are used for the downscaling: topographic data from the HydroSHEDS database (SRTM SAR derived) and Sentinel-1 SAR images. The HydroSHEDS database is provided at different spatial resolutions, the highest being 3 arcsec (i.e. about 90 m at the equator), which approximately corresponds to the level-1 GRD medium resolution of S1 SAR images. The HydroSHEDS database is organized as 5° latitude - 5° longitude tiles (36 millions of pixels) at the global scale. Considering the size of high resolution global datasets, the same structure and resolution will be used to downscale the GIEMS product.

As stated previously, two methods are proposed to derive the floodability index. The first one is based on topographic characteristics and has the advantage of being easily applicable at the global scale. The second one is based on inundation observations and is then undoubtedly more precise but it also requires multiple observations of the same region and cannot be easily applied at the global scale due to data availability. In the following, both methods are explained in details.

3.2 Topography-based floodability index

The first method to derive the floodability index relies on the assumption that the flood dynamics is mainly driven by topographic characteristics, such as slope or distance to rivers (Fluet-Chouinard et al., 2015). The HydroSHEDS database has been used to derive a panel of different topographic indices as listed below. Then a neural network algorithm has been set up in order to extract the most relevant indices and compute the floodability index.

3.2.1 Topographic indices

To derive topographic indices, we considered the HydroSHEDS dataset (Hydrological data and maps based on SHuttle Elevation Derivatives at multiple Scales), which is widely used in the hydrology community. HydroSHEDS provides hydrological information in a coherent format at the global scale (Lehner et al., 2006), including elevation, drainage network, flow direction and accumulation. This database is derived from the Shuttle Radar Topography Mission (SRTM) at a 3'' resolution (90 m).

It also provides a corrected DEM, called conditioned DEM, based on hydrological constraints (void-filling and river network consistency). Also, mean river discharge data provided by Bernard Lehner have been used to define rivers and their size. The corrected DEM and the drainage directions have been used to derive the following topographic indices:

- drainage network distance to river: this is the distance (in number of pixels) following the drainage network to the closest river;

- straight line distance to river: this is the distance (in metres) to the closest river;

- elevation from river: this the elevation of the pixel with respect to the closest river;

- slope: this is the slope (in m/m) along the drainage direction.

For the first three indices, different discharge thresholds have been used to define small, medium and large rivers: 500, 10 000 and 100 000 m3/s. Consequently, a panel of 11 topographic indices (including slope and mean discharge) has been computed for each HR pixel of the globe.

3.2.2 Neural Network approach

In order to find the most relevant topographic indices and their relationship with inundation spatial structures, a neural network approach has been set up. The idea is to find statistical relationships between the different topographic indices and flooded pixels. The method then requires a reference inundation map. A Sentinel-1 SAR-derived inundation map is a good candidate but it would require a sample of Sentinel-1 SAR inundation retrievals all around the world to represent all types of inundations states, which is not available yet. Instead, we used the Global Lakes and Wetlands Database (GLWD, Lehner and Döll, 2004) that combines a variety of existing global lake and wetland maps into one consistent coverage. GLWD represents a comprehensive dataset of global surface water area, including small and large lakes, reservoirs, smaller water bodies, rivers, and a good representation of the maximum global wetland extent. It is considered to be the best available water mask of its kind, see Nakaegawa (2012). The level 3 GLWD dataset is provided at the 30 arcsec resolution and it has first been downscaled to the 3 arcsec resolution for compatibilities with the HydroSHEDS data. It should be noted that as soon as SAR retrievals from Sentinel-1 will be made available at a larger scale, GLWD database could be replaced by these new estimates to develop a better neural network SAR retrieval. The LandCover_cci Water Bodies product could also have been an interesting alternative. It is derived from the ENVISAT-ASAR dataset and represents permanent open water bodies at a 300 m resolution. Since this dataset is based on SAR retrievals, it has been decided not to use it in order to prevent any redundancy between the topography- and SAR-based methods and keep them as independent as possible. Nevertheless, the use of SAR-based water maps as a reference for the topography-based floodability index is seen as a perspective of coupling both methods.

The neural network takes topographic indices as inputs and provides floodability indices as outputs. To train the neural network, a random sample of pixels is first created. Worldwide pixels are selected randomly, but, given that the large majority of pixels are not flooded, we paid careful attention to include 50 % of flooded pixels. Several tests have been conducted including different sets of topographic indices. More details of the derivation of topography-based floodability indices and the downscaling algorithm can be found in Miolane et al. (2016, to be submitted) and will not be reported here. Namely, the authors present a sensitivity analysis of the floodability index to the different topographic indices, as well as a smoothing procedure between GIEMS cells. The downscaling method is applied on the GIEMS product at the global scale over the whole time period (1993-2007) and evaluated over the Amazon Basin and the Niger Inner Delta. This is an extension of the work performed by Fluet-Chouinard et al. (2015).

Again, this approach could be improved if SAR reference inundation maps were available at the global scale. Several zones covering different topographic and hydro-climatic conditions should be available in order to create a reliable sample. This option is seen as a perspective of the current work that will be possible when the SAR community provides an operational SAR inundation estimates.

3.3 Observation-based floodability index

The second method to derive the floodability index is based on satellite observations only. More specifically, several inundation maps at high resolution are used to define an inundation frequency for each HR pixel. This method is expected to be more accurate if the original HR dataset is of enough quality because it does not rely on topographic indices only; however it is sensitive to problems in satellite measurements (presence of vegetation or clouds, atmospheric corrections, etc.). Furthermore, it requires at least a whole season of observations with minimum and maximum flood extents, and ideally several years of observations to provide reliable seasonal statistics. A practical difficulty of this method is that no high resolution dataset of flood extent dynamics still exists at the global scale. Indeed, despite recent studies showing the potential of satellite observations to derive inundation maps over specific regions, the processing methodologies cannot be easily extended at the global scale.

In this project, a portion of the Danube Basin has been selected to study the efficiency of the downscaling method based on Sentinel-1 SAR images (Fig. 1). SAR images from Sentinel-1 are available over this region since October 2014 with a 12-days repetitivity (6-days when Sentinel-1B will be available). Nevertheless, deriving inundation maps from SAR backscatter maps is not straightforward and an important part of this work was dedicated to that, as detailed in the next section.

Inundation maps derived from Sentinel-1 SAR observations are then used to compute the floodability index (as the inundation frequency of each HR pixel). Lastly, the same downscaling methodology as for the topography-based floodability index (see above and Miolane et al., 2016) is applied on the GIEMS product over the study zone and for the whole time period (1993-2007).

4 Water detection from Sentinel-1 SAR observations

4.1 Overall methodology

This section describes the methodology to extract water maps from Sentinel-1 SAR observations. Sentinel-1 SAR observations consist in backscatter coefficients given in two polarizations: VH and VV. The backscatter coefficient is usually a good indicator for detecting water since it shows very low values over water pixels. One of the main advantages of using SAR observations to detect water is that observations are available day and night and whatever the meteorological conditions (not sensitive to clouds). Nevertheless, discriminating water from land is not straightforward and a simple threshold value does generally not guarantee accurate water detection. The idea here is to use Landsat-8 imagery within a neural network approach to transform Sentinel-1 observations into water maps. Cloud free Landsat-8 images are first gathered, with dates corresponding to available Sentinel-1 observations (+ or – 7 days). These images are used as a reference to train a neural network over Sentinel-1 data. This neural network is then applied on all available Sentinel-1 observations.

4.2 Sentinel-1 SAR data

Sentinel-1 data are provided by ESA. Level -1 data are freely available on the Sentinels Scientific Data HUB (https://scihub.copernicus.eu/). Here, Interferometric Wide swath (IW) mode is used, with a 250 km swath at 5 m by 20 m spatial resolution and a 12-day repeat cycle at Equator (one satellite).

Level-1 Ground Range Detected (GRD) data with relative orbit 73 and slice 11 and 12 were downloaded for the period October 2014 to February 2016, representing 60 images for about 66 GB.

All these images were first pre-processed, including calibration, speckle filtering and terrain correction. These steps are performed using the ESA Sentinel tool called SNAP. The calibration consists in converting digital numbers (integers) stored in the image files into backscatter intensity (Sigma_0) in both dual polarisation (VH and VV). The speckle filtering is used to remove the speckle noise. It basically consists in an averaging window, but more sophisticated filters are available. For instance, the "refined Lee" filter uses the variance around a pixel and is preferred to preserve edge shapes (such as roads, rivers, etc.). The latter was used in this study with an edge threshold of 5000. Finally, the terrain correction is used to correct distortions due to geometry and terrain elevation. By default, the SRTM at 3sec resolution is used as the reference DEM. After the terrain correction step, the final image is projected on the geographic reference WGS84 (latitude-longitude) and upscaled to the HydroSHEDS resolution. Note that the upscaling to the HydroSHEDS resolution is not necessary and was done here for comparisons between the two methods (topography- and SAR-based floodability indices). A higher resolution could have been chosen, such as the resolution of Landsat-8 images used as reference inundation maps.

4.3 Landsat-8 data and water mask

Landsat-8 provides images in the visible and infrared bands at a spatial resolution of about 30 m, which is of particular interest to compute the Normalized Difference Vegetation Index (NDVI) often used efficiently to discriminate water from land. With the recent launch of Sentinel-2 (June 2015), higher resolution images are now available to compute the NDVI (up to 10m). Sentinel-2 data were not used in this study because the overlapping period with Sentinel-1 was too short.

Landsat-8 data are freely available at different places. Here Landsat-8 scenes were ordered from the USGS web site (http://espa.cr.usgs.gov/) where high level products (such as surface reflectance or NDVI) are proposed, as well as reprojection and resampling processes. Bands 4 and 5 are required to compute the NDVI. The data from the original product may be used to compute (quite easily) the Top of Atmosphere (TOA) reflectance. Surface reflectance can be obtained after performing an atmospheric correction. Even though using TOA reflectance can satisfactorily discriminate water from land (see e.g. Parente, 2013), using surface reflectance is more rigorous, all the more so as it is provided by USGS.

4.3.1 Cloud and snow mask

Cloud and snow pixels have to be filtered from the Landsat-8 image. A quality assessment (QA) file is provided along with the original images, including cloud and snow confidence flags. Another option is to use the cfmask file from USGS, which is proposed along with the surface reflectance bands and NDVI. USGS applied a specific algorithm to detect clouds and snow (Zhu and Woodcock, 2012). There are some noticeable differences between both cloud masks (from the QA file and cfmask), as shown in the following figure:

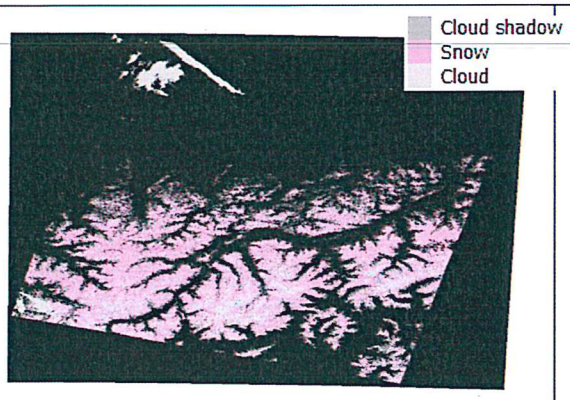

Cloud and snow cover from QA file

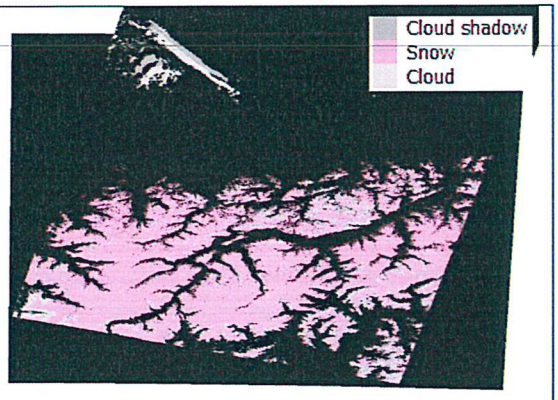

Cloud and snow cover from cfmask (USGS)

Fig. 2. Cloud and snow cover from Landsat-8 with two different algorithms.

4.3.2 Water map

At this stage, there are three options to map water from Landsat-8 images. The first one is to compute TOA NDVI and classify water pixels where NDVI < 0 and land pixels where NDVI > 0. The second option consists in using surface reflectance instead of TOA. The third option is to directly use the water classification from the cfmask file. In this file, a water test is used to improve cloud detection (Zhu and Woodcock, 2012). This test is based on both NDVI and Band 4 (red):

$$\text{Water Test} = (\text{NDVI} < 0.01 \text{ and Band } 4 < 0.11) \text{ or } (\text{NDVI} < 0.1 \text{ and Band } 4 < 0.05).$$

From Fig. 3, it seems that the water test done in the cfmask algorithm works better than the two others. Since this file is already generated by USGS, at different possible resolution, and that it also includes cloud and snow flags, it would be the most convenient way to extract water maps from L8 images.

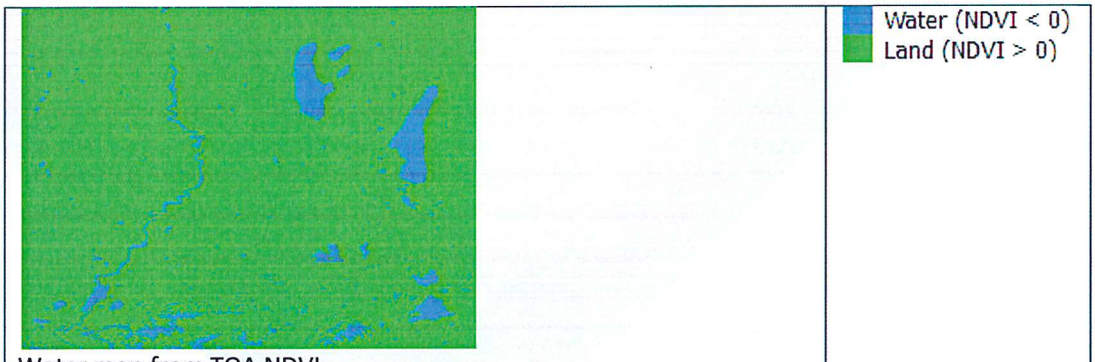

Water map from TOA NDVI

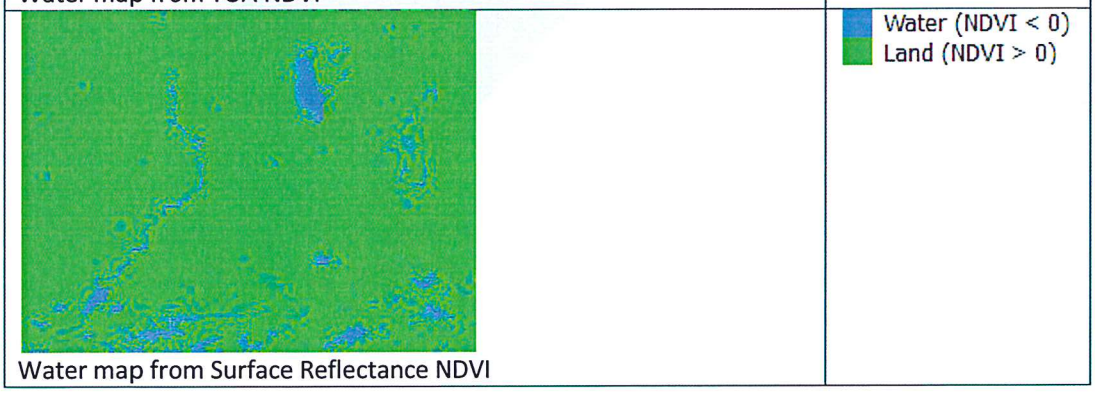

Water map from Surface Reflectance NDVI

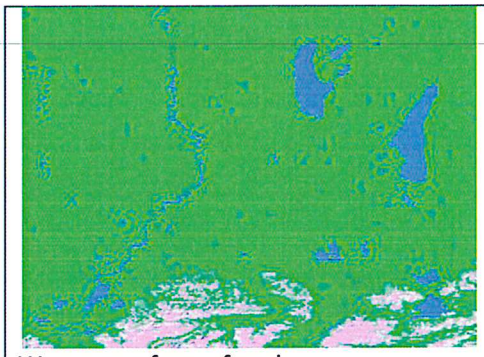

Water map from cfmask

Fig. 3. Water classification from Landsat-8

4.4 Neural Network

In order to train the neural network to extract water maps from Sentinel-1 data, Landsat-8 water maps are used and must be resampled at the same spatial resolution. Since the final resolution is the one of HydroSHEDS (3arcsec), both Landsat-8 and Sentinel-1 have been resampled at this resolution. Several upscaling algorithms may be tested, including, e.g., nearest neighbour, window average or 5th percentile. Only the first option is explored here.

4.4.1 Neural network training

The first step is to extract pixels available in both Sentinel-1 and Landsat-8 images. Then Sentinel-1 data are converted into decibel values (it is better to convert to dB after any processing so that resampling is applied on real values). A sample of pixels is chosen randomly among the available pixels. Among all the pixels within an image, a very small percentage are flooded, most of them being land. In order to improve the efficiency of the neural network training, 25 % of the sample gathers water pixels and 75 % gathers land pixels. Different sample sizes have been tested, and the optimal value was 100,000 pixels which is the size chosen in the following tests. The sample pixels are extracted from 5 Landsat-8 and Sentinel-1 images with close dates (+ or – 7 days, see Fig. 4).

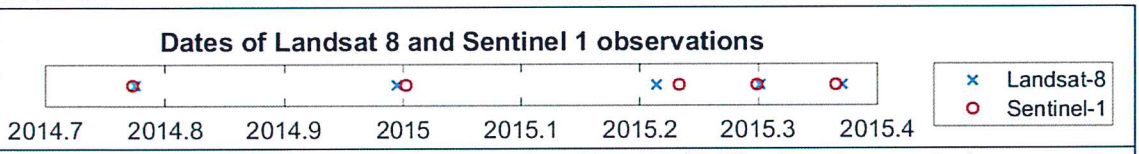

Fig. 4. Dates of Landsat-8 and Sentinel-1 images used for the classification of water pixels.

The neural network is used to transform the backscatter coefficients from Sentinel-1 into values between 0 and 1 that can be interpreted as the probability of each pixel to be inundated (kind of floodability index). The inputs of the neural network are the backscatter coefficients in both dual-polarisation (Sigma0_VH and Sigma0_VV). The targets are the water flag from Landsat-8 images and the output are values ranging between 0 and 1, marked as water if greater than 0.5 and as land if lower than 0.5. As shown on Fig. 5, the confusion matrix shows overall good results with a high global accuracy (more than 90 %).

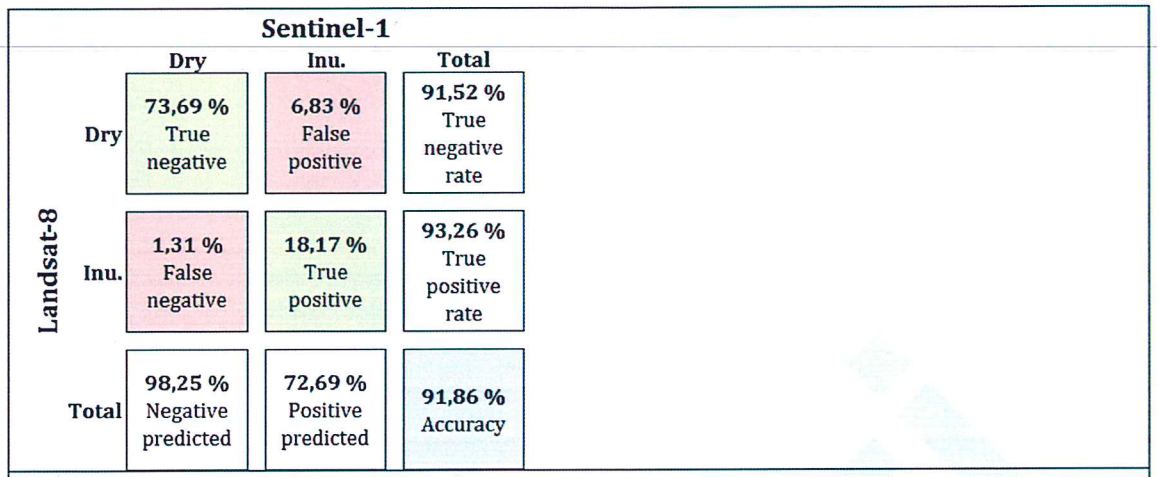

Fig. 5. Confusion matrix for the Sentinel-1 training.

It could be possible to improve this results by including other potentially relevant values into the training, such as the minimum, maximum, temporal average and standard deviation of the backscatter coefficient, as well as the spatial standard deviation (over a 9-pixels size window). The first four values are computed using all the available Sentinel-1 observations, whereas the spatial standard deviation is computed for each image (each date) independently. All the derived values are computed for both dual polarisations, so that 10 values are available for each pixel. All the possible combinations of different values have been tested and results are reported in Table 1. For each combination, both polarisation (VH and VV) are considered.

1	2	3	4	5
Sigma_0	spatial var (9)	minimum	maximum	temporal std

	target=0	target=1	output=0	output=1	overall
1	98.2401	72.7276	91.5301	93.2319	91.8620
2	96.6105	67.6520	89.9596	86.9335	89.3709
3	99.2267	77.6686	93.0214	97.0999	93.8370
4	99.4559	70.7766	90.9865	97.7707	92.2248
5	97.2279	65.4990	89.4225	88.7338	89.2954
1-2	98.6676	75.8872	92.4675	94.9963	92.9725
1-3	99.3710	77.6390	93.0223	97.6273	93.9378
1-4	99.3693	74.9166	92.1570	97.5638	93.2038
1-5	99.1378	74.7244	92.1669	96.6543	93.0343
2-3	99.3719	79.2719	93.4988	97.6784	94.3468
2-4	99.1474	76.3661	92.5613	96.7946	93.4034
2-5	97.7584	75.1588	92.1909	91.7878	92.1084
3-4	99.3944	78.3137	93.1481	97.7577	94.0792
3-5	99.3431	77.7330	93.0478	97.5277	93.9404
4-5	99.4082	78.7571	93.2796	97.8197	94.2013
1-2-3	99.1699	78.9915	93.4041	96.9439	94.1252
1-2-4	99.1740	77.2833	92.8310	96.9272	93.6545
1-2-5	99.2311	77.9266	93.0968	97.1252	93.9048
1-3-4	99.3604	78.3849	93.1668	97.6371	94.0717
1-3-5	99.3990	77.8498	93.0853	97.7365	94.0116
1-4-5	99.4292	78.6236	93.2416	97.8920	94.1833
2-3-4	99.3788	79.9016	93.6168	97.7461	94.4679
2-3-5	99.3946	79.2055	93.4807	97.7585	94.3472
2-4-5	99.4575	79.8959	93.6199	98.0259	94.5253
3-4-5	99.4779	78.8514	93.3118	98.0738	94.2771
1-2-3-4	99.4194	79.7406	93.5714	97.8859	94.4576
1-2-3-5	99.4375	79.3151	93.5154	97.9170	94.4068
1-2-4-5	99.2707	79.5136	93.4950	97.3515	94.2892
1-3-4-5	99.3372	78.6386	93.2401	97.5612	94.1183
2-3-4-5	99.4386	80.0274	93.6578	97.9616	94.5443
1-2-3-4-5	99.3791	80.0744	93.6682	97.7519	94.5117

Table 1. Performances of the different combinations for the neural network training (target is Landsat-8, output is Sentinel-1).

First, it is clear that the minimum and maximum backscatter values are the two indices with the best performances. Then, increasing the number of indices generally improves the performances, with an overall accuracy reaching 94 %. Nevertheless, results could be somewhat different with a longer time series or in different environment (hydroclimatic conditions). In the following, we preferred to use the five indices.

4.4.2 Sentinel-1 water classification

The neural network being trained, it is possible to apply it on all the available Sentinel-1 observations. Fig. 6 shows the comparison between Landsat-8 water mask (20th March 2015) and Sentinel-1 water probability (27th March 2015), i.e. output of the neural network, over two different regions.

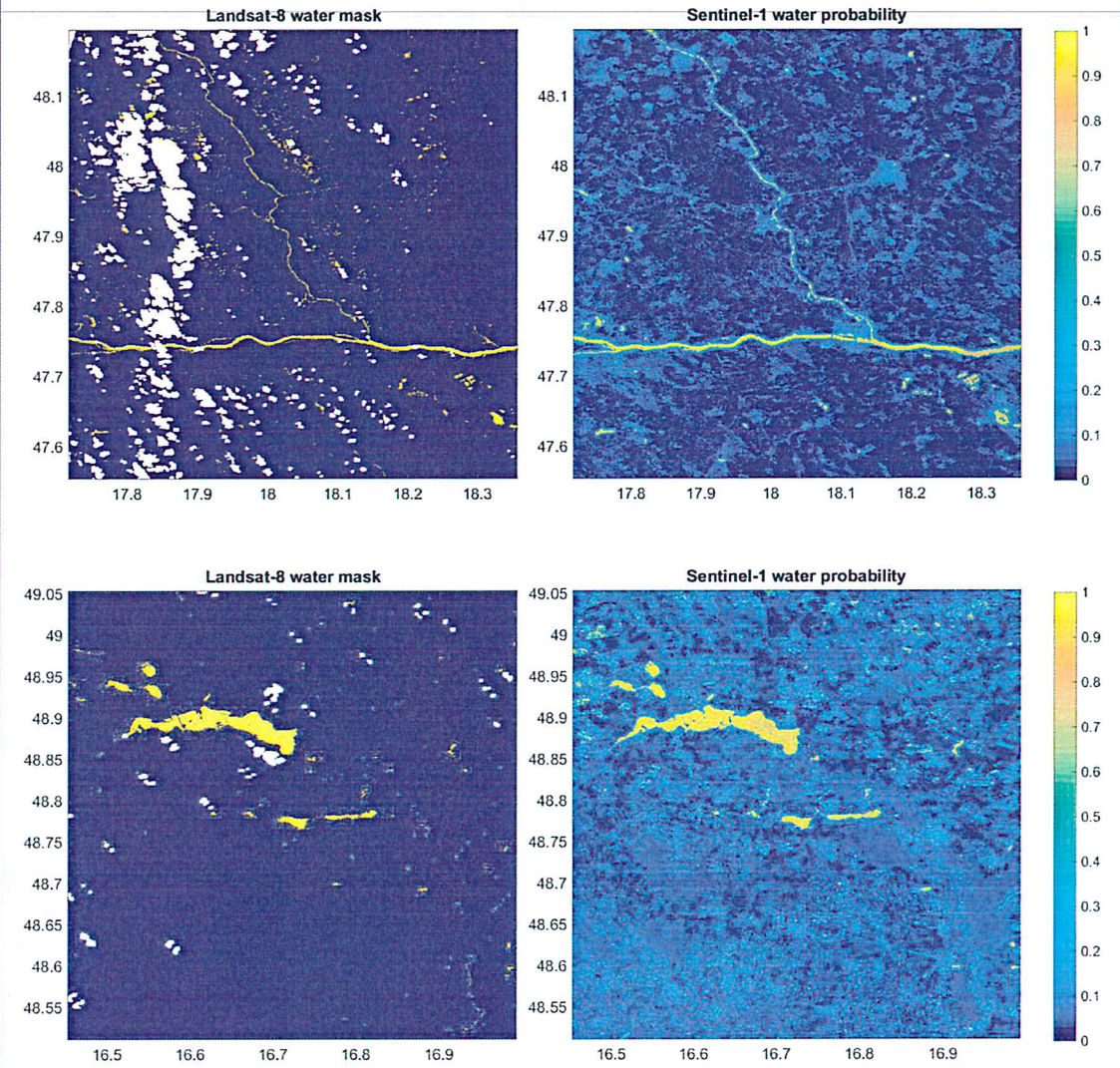

Fig. 6. Landsat-8 water mask and Sentinel-1 water probability (25th July 2015).

The Sentinel-1 water detection algorithm clearly detects the main water structures, such as main rivers and lakes as well as small water bodies. Besides, Sentinel-1 also detected small structures such as fields, with a non negligible water probability. This means that such fields would be potentially flooded during the downscaling process if enough water is available within the corresponding low-resolution GIEMS pixel.

4.4.3 Comparison with topography-based floodability index

Fig. 7 shows the comparison of the floodability index computed from Sentinel-1 SAR data or topography indices over the considered region and two different small zones. As shown in the left column, the contrast between always flooded pixels (rivers, lakes) and the other ones is very high. To enhance the colours and the spatial structures of the floodability index, a CDF (Cumulative Distribution Function) matching method has been applied, with the topography-based floodability index as a reference (see Fig. 8). The CDF matching has no impact on the downscaling procedure since the pixel hierarchy (in terms of floodability index values), that is used in the downscaling process, is not changed.

It is clear that the main water bodies such as large rivers and lakes are well represented by the floodability index in both cases (values close to 1). Small details such as the braided part in the middle zone of the third line seem to be better represented by the SAR method, as well as some flooding zone (see e.g. the eastern part of the river in the middle line, or the north-western part in the third line). The area surrounding the lake (middle line in Fig. 7) also shows high floodability values with the SAR method, meaning that it would be flooded during rainy events. The topography method shows the same behaviour, which corresponds to increasing lake extent due to topography that happens when the lake level increases. In the topography method regions with the highest floodability indices are located near permanent water bodies (rivers and lakes). The floodability spatial structure for the SAR method is very different, showing high floodability over fields rather than near rivers (see also Fig. 9). For quite flat regions, the topography method cannot attribute high priority to fields and tends to prioritize river banks. Since the SAR method is based on observations, it is expected to be more reliable.

On the other hand, some rivers that are clearly visible in the topography method do not appear as probable flooded pixels in the SAR method. The most probable reason is that these are small rivers that have been enhanced by the topography-based procedure and minimized by the SAR-based method because of the Sentinel-1 upscaling step, as shown on Fig. 10. It should also be noted that potentially inundated pixels might not be indicated by the SAR floodability index because they have not been inundated during the period used to define the SAR floodability. For instance, a large and extreme inundation pattern occurring only one time per decade would not be represented in the SAR time record used to define the floodability index, but it might be present in the topography index.

Finally, Fig. 8 shows a quite binary behaviour of the CDF of the SAR-based floodability index. This means that wetted pixels were inundated in almost all SAR images, or in other words, that the temporal variability of the flood extent was quite low during the observation time span. Indeed, the year 2015 was quite dry in most of the European basins. This is a limitation of the SAR method. Its performances would increase with a longer time series, especially if images capture various inundation states.

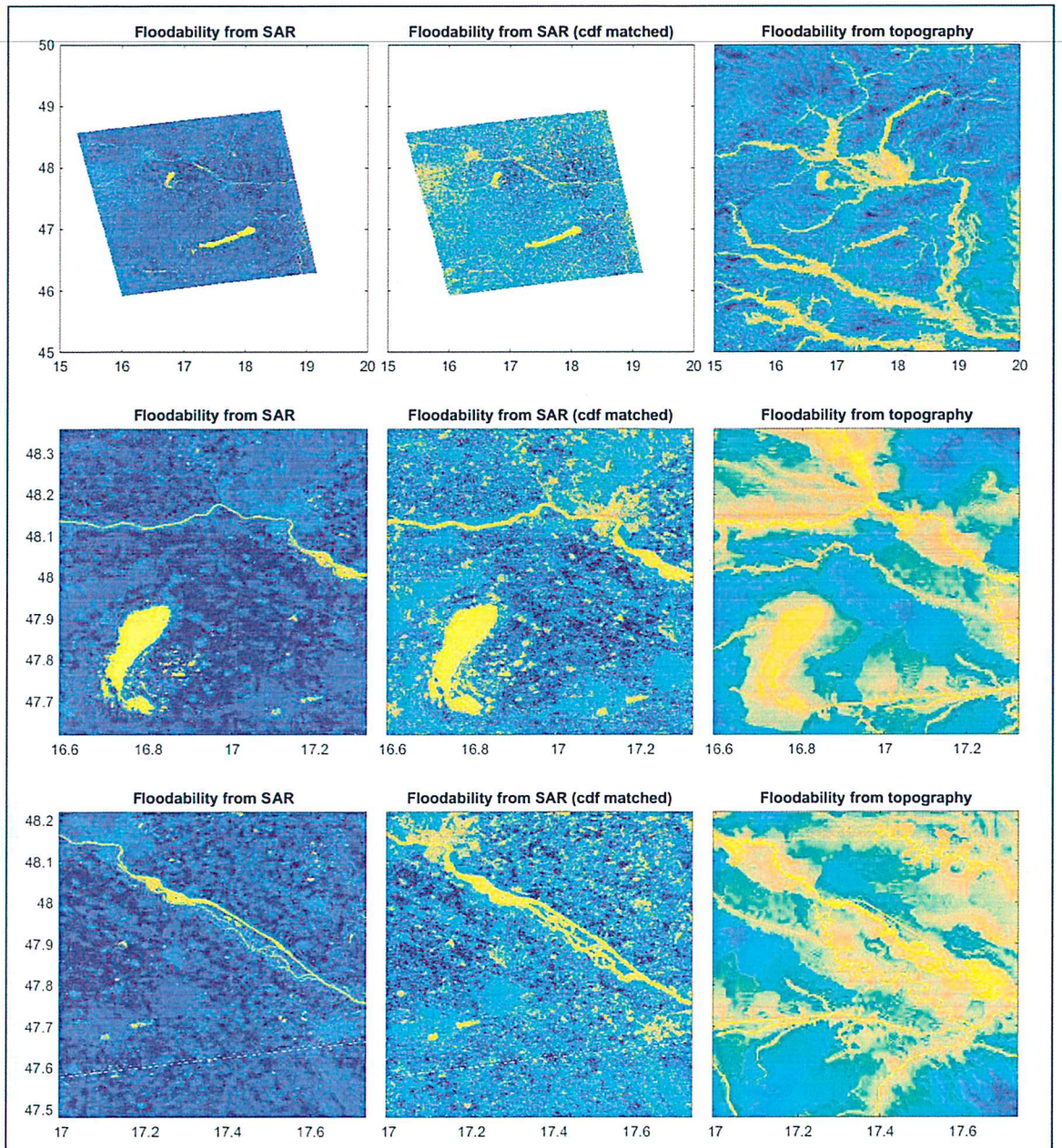

Fig. 7. Comparison of the floodability index computed from Sentinel-1 SAR data or topography indices. The column in the middle corresponds to a CDF matching of the first column to enhance colours for a better comparison.

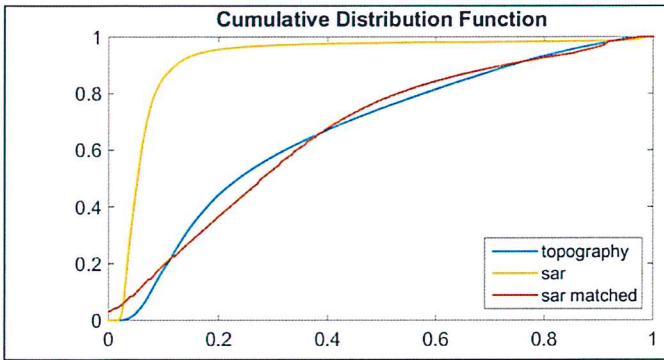

Fig. 8. CDF matching of the SAR-based floodability index (non inundated pixels have been removed).

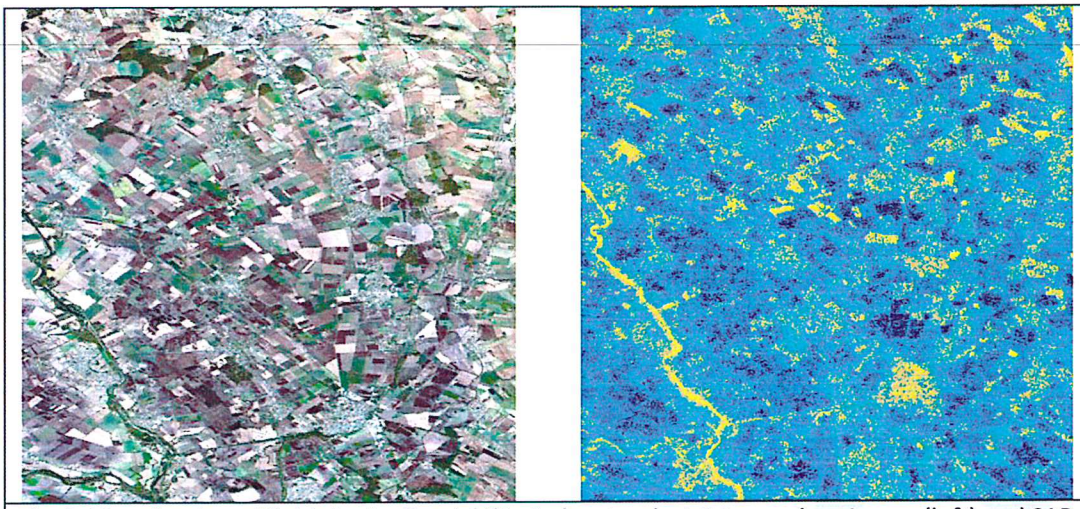

Fig. 9. Visualization of fields in the floodability index. Landsat-8 true colour image (left) and SAR-based floodability index (right).

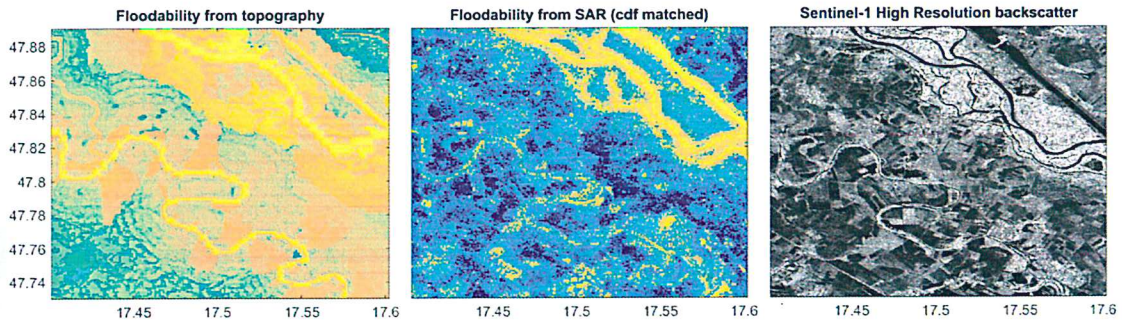

Fig. 10. While small rivers are enhanced by the topography method (left), they are not well captured by the SAR method (middle), even though they are quite visible in the 10 m high resolution Sentinel-1 image (right).

5 Downscaling of the GIEMS product

The method to downscale the GIEMS product from the floodability index is described in section 3 and more details can be found in Miolane et al. (2016, to be submitted). The GIEMS product has been downscaled at the global scale and over the whole time span (1993-2007) using the topography method. On the other hand, the SAR method has been used to downscale the GIEMS product over 1993-2007 for the considered region in the Danube basin. Both methods are compared in the following sections.

5.1 Downscaled product at different time steps

Fig. 11 and Fig. 12 show the comparison between the topography- and the SAR-based methods at different time steps and over two sub-regions. The original low-resolution GIEMS product is represented as blue shading background (with a different colour scale). Three time steps are represented, the first one corresponding to the minimum flood extent, the third one to the maximum and the second one to an intermediate situation.

Differences between both methods only rely on differences between floodability indices. Consequently, all the similarities and differences raised in the previous section are also visible in the downscaled product. Namely, as shown on the low flow time step (first line), the main water bodies (rivers and lakes) are well represented. The GIEMS-SAR product seems to be finer in the details but some small rivers are missing. Instead, small water bodies and flooded river banks are present in the GIEMS-SAR product. Besides, the topography method shows some artefacts in lakes because the HydroSHEDS database represents the bathymetry instead of a flat region over large lakes (based on the SRTM Digital Elevation Model).

When the water extent increases, flooded areas are concentrated near the rivers with the topography method, whereas the SAR method tends to inundate small bodies such as fields and small lakes and to slightly increase the river width. This is due to the high importance of the distance to river information in the floodability index with the topography method. In Fig. 12, the lake extent exaggeratedly increases at very high flow with the topography method, as well as river width. It is more likely that fields and small water bodies become inundated in such a situation. No images were available at this resolution and time steps, so that validation is quite difficult, all the more so as no major flood event occurred over this region during the Sentinel-1 time span (from October 2014). Nevertheless, the SAR method seems to be more realistic. Advantages and drawbacks of both methods are detailed in the Discussion section.

5.2 Temporal statistics

Fig. 13 and Fig. 14 show the number of flooded months and the inundation variability (in terms of standard deviation) over the whole time period (180 months) for both methods. As stated previously, all the inundated areas are located near rivers with the topography method, then showing a high temporal variability. On the contrary, with the SAR method, only a few pixels on the river sides and around the lake show high temporal variability. The flooded zones are more diffuse and mainly represent fields and small lakes. One may also notice that the variability is quite high in towns, as in Bratislava (North-East of the lake in the second line). Even though major floods occurred during this time period in Bratislava (e.g. in August 2002), the high value of the standard deviation may be partly due to misclassification errors during the Sentinel-1 neural network training. To overcome this issue, it could be possible to use ancillary data (such as land cover classification) to force urban zones to be set to dry pixels. Overall, the GIEMS-SAR downscaled product shows a satisfactorily temporal and spatial behaviour, and seems to improve the topography-based product. Note that the inundation variability within the lake with the topography method is due to non uniform lake topography in HydroSHEDS (which is necessary in hydrological applications to ensure flow routing throughout the lake).

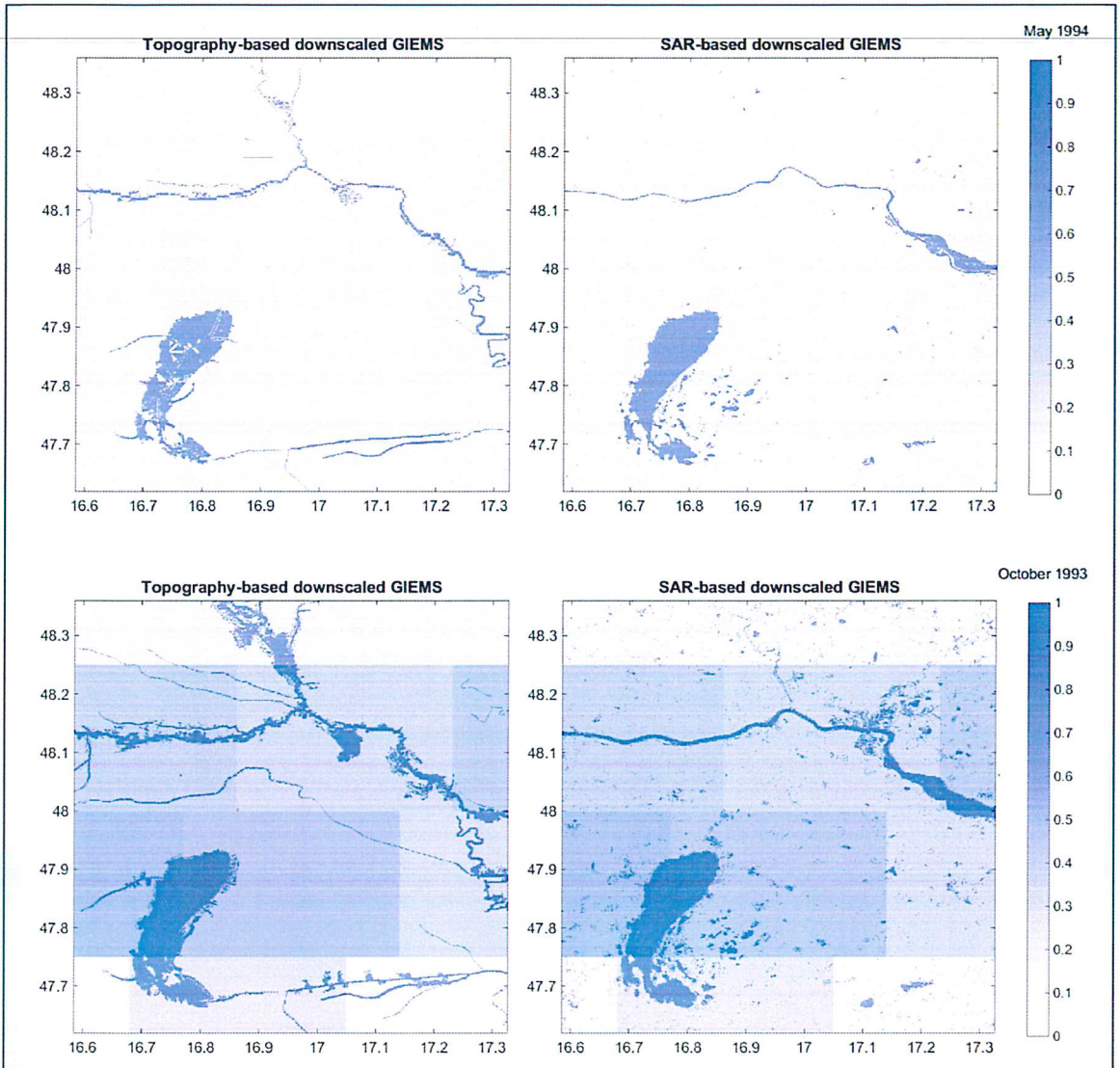

Fig. 11. Comparison between topography- and SAR-based downscaling methods at different time steps. The background blue shading represents the original GIEMS product.

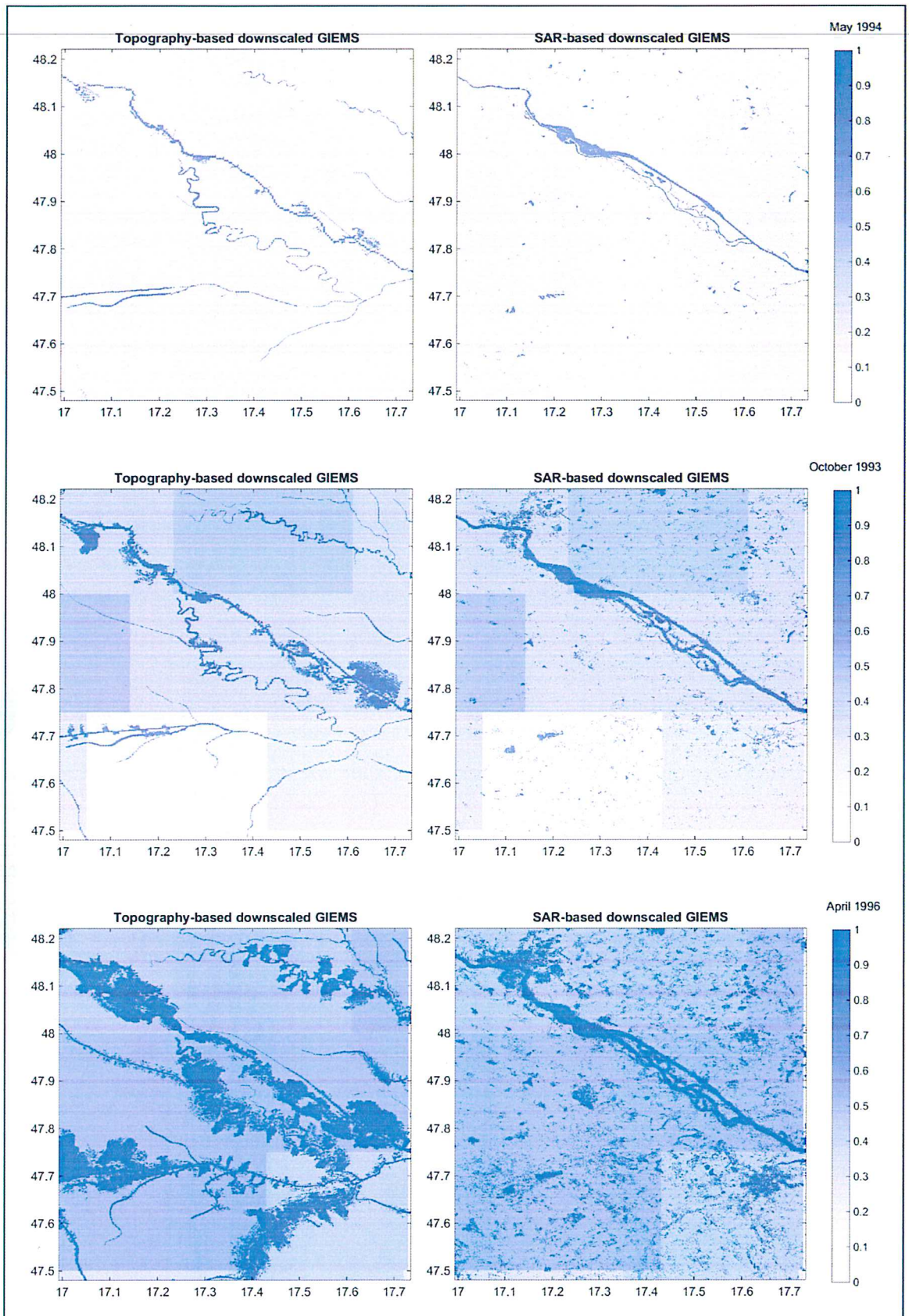

Fig. 12. Same as Fig. 11 for a different zone.

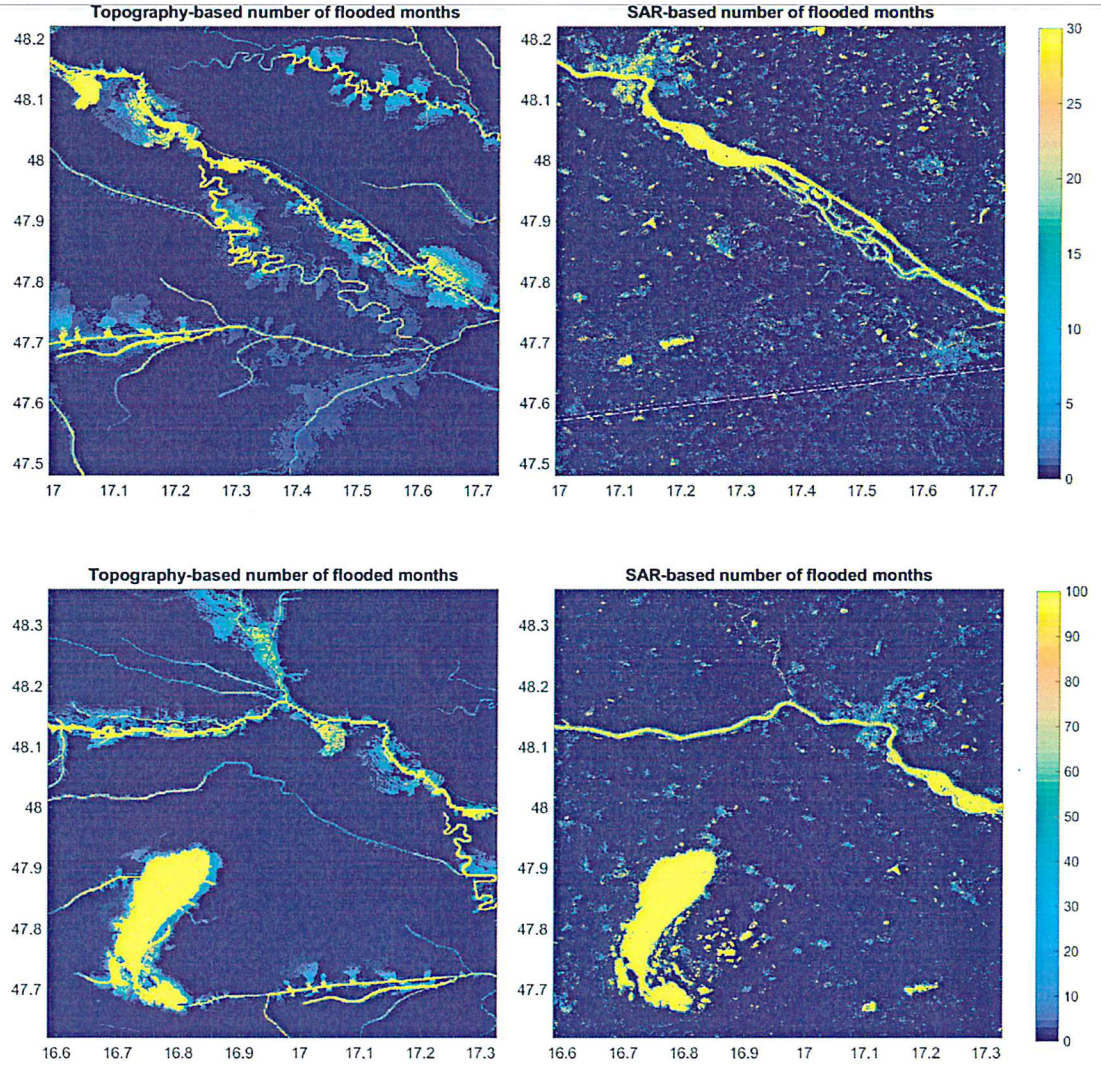

Fig. 13. Number of flooded month per pixel over 1993-2007 for the topography- and SAR-based methods. Images joins in the upper right figure appeared due to border effects during the resampling process.

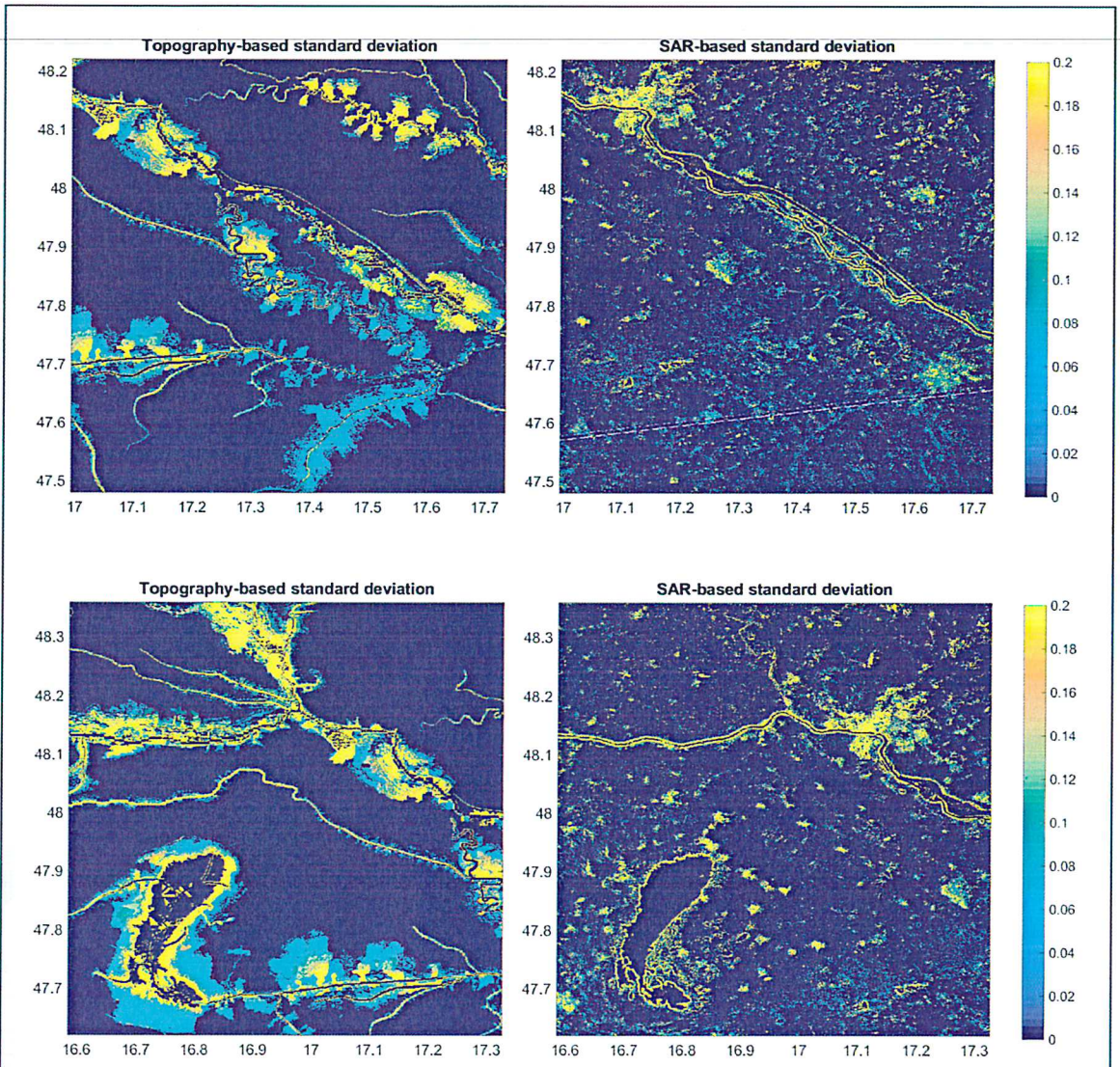

Fig. 14. Inundation variability (standard deviation) over 1993-2007 for the topography- and SAR-based methods.

6 Discussion and perspectives

6.1 Discussion

This project focused on the development of methodologies to downscale the GIEMS product. GIEMS is a global scale dataset based on multi-satellite observations and consists in monthly maps of water surface extent at the 0.25 degree spatial resolution. Downscaling GIEMS to resolutions of about 100 m would allow the observation of the dynamics of about 80 % of surface water around the world over the last two decades. Such a dataset would be very valuable for a wide range of studies, from local hydrology (high-resolution) to climate (long time series) where surface water is a key component. Namely, the surface water component in the water and biochemical cycles is one of the most directly impacted by human activities, and characterising it globally, at high resolution and over a long time period is essential to better understand the causes and consequences of Climate Change.

Two methodologies have been proposed, both based on the computation of a floodability index representing the probability of each high-resolution (HR) pixel inside a low-resolution (LR, the GIEMS resolution) pixel to be flooded. The first method relies on a panel of topography indices (elevation, slope, distance to river, etc.) computed from the HydroSHEDS database. Its main advantage is that it can more easily be extended at the global scale. The second method is based on satellite SAR observations from the Sentinel-1 mission. Contrarily to the topography method, it is based on observed inundation maps and consequently accounts for flooding that is no only topography-related (such as anthropogenic structures or irrigation). The major drawback of this method is the requirement of long time series of HR observation-based water maps. Despite the increasing number of satellite observations, deriving HR water maps is not straightforward at the global scale and requires a large amount of resources (storage and CPU) and reliable retrieval algorithms effective on diverse environments. As a consequence, great efforts are still needed to perform a global scale downscaling with this method. As stated thereafter, combining both methods could represent an interesting alternative.

The topography-based method has been applied at the global scale to derive the floodability index for each land pixel at the 90 m spatial resolution (resolution of HydroSHEDS). In this project, for the SAR-based method, a first step has been to develop algorithms to derive water maps from backscatter SAR observations. A Neural Network approach has been defined, using Landsat-8 images as a reference. One may note that Landsat-8 images could have been used directly to derive the floodability index, but such observations are highly sensitive to meteorological conditions (clouds), and it is almost impossible to get a complete hydrological season. The SAR Neural Network retrieval is able to extend temporally and spatially the clear sky inundations estimates of Landsat, even for cloudy scenes. Different options have been tested for the neural network training, including the consideration of different indices derived from the backscatter coefficient (extreme values, spatial and temporal standard deviation) or the percentage of flooded pixels in the training sample and the upscaling resampling method. When compared to Landsat-8 water maps, the method provided good results, with an overall accuracy higher than 90 %. The floodability index has then been computed using the output of the neural network applied at each time step and for each pixel.

Different comparisons between the topography- and the SAR-based methods have been performed, in terms of floodability index and spatio-temporal of the downscaled GIEMS product. Both methods show overall good results, with a satisfactory detection of permanent water bodies. This result is quite obvious for the topography method since the neural network used to set up the floodability index uses the Global Lakes and Wetland Database (GLWD) as a reference. As a consequence, the distance to river topographic index has a large weight in the neural network and pixels near the main rivers show high floodability indices. For the SAR-based method, the good detection of main water bodies is representative of the good performance of the water map extraction from Sentinel-1 observations. It has to be noticed that some rivers detected by the topography method (actually present in GLWD) are not detected by the methodology used with Sentinel-1. Reasons could be the small size of these rivers or misclassification errors. To confirm the former, tests at a higher spatial resolution (e.g., the original Sentinel-1 resolution) could be performed, for instance at the Landsat-8 resolution, or even higher when enough Sentinel-2 images will be available.

Another consequence to the use of GLWD as a reference for the topography method (and the large weight of the distance to river topographic index) is that the highest floodability values, after permanent bodies themselves, are located near the rivers and the lakes, while the plains show very low values. Hence, with the topography method, floods mainly occur near the river, leading to

unrealistic river widths or lake surface extents. On the contrary, the SAR method, which is only based on observations, shows a more diffuse spatial pattern, with narrow flooded areas in the rivers sides and a lot of small water bodies within the plains, corresponding to flooded fields and small lakes. The SAR-based method seems to provide more realistic spatial and temporal characteristics of the flood dynamics, which should be validated in the future with independent observations.

To summarize, the topography-based method can be easily applied at the global scale, whereas the SAR-based method requires a large amount of data and reliable retrieval algorithms. Moreover, the SAR method is limited by the available observations (the length of the time series and the observed variability); potentially flooded pixels may never be inundated if they were not inundated in any of the SAR observations. As a perspective, other SAR-based observations could be used to extend the time period (such as PALSAR, PALSAR-2, ERS-1 and 2 or ASAR). On the contrary, the topography method creates a complete hierarchy of all the pixels, which enables any pixel to be inundated. On the other hand, the topography method is limited to topographic indicators, while the SAR method is based on observation and can then account for isolated small water bodies and zones affected by human activity that would not be seen by the topography method. Potential combinations of both methods are quickly explored in the next section.

6.2 Future work

As potential future work, some technical analyses should be performed in order to improve the results or assess the impact of some aspects of the methodology. Namely, the impact of the speckle noise inherent to SAR observations is not clearly assessed and may be responsible for misclassifications errors in the development of water maps from Sentinel-1 (e.g. in urban regions). This would directly impact the floodability index and therefore the downscaled results. Larger time series would dampen the importance of the speckle errors. Different speckle filters could be tested, including more sophisticated ones such as multitemporal filters.

Also, a comprehensive analysis of the impact of the spatial resolution is recommended. In this work, the HydroSHEDS database was used to develop the topography-based floodability index and its spatial resolution (3 arcsec, or about 90 m at the Equator) was chosen for the final product. Nevertheless, different products with different spatial resolution were used as well: the GLWD database, Landsat-8 images and of course Sentinel-1 observations. Each dataset has been resampled at the final resolution. Even though different resampling techniques have been tested, other techniques could provide significant improvements. Also the final resolution in this study is not the original resolution of Sentinel-1, and potential of this highest resolution on the downscaling performance could be explored. Besides, the time period in this study was quite short (about 1.5 years), limiting the number of observed flood events. The performances of the GIEMS downscaling highly depend on the variability (in space and time) of the inundated pixels. Hence a comprehensive sensitivity analysis of the length of the study period could be performed.

Another perspective is the development of a seasonal floodability index. The idea is to use different indices depending on the season, considering that the inundation dynamics can vary during the year. To do so, several years of SAR observations are recommended in order to set up 3-monthly seasonal floodability indices. The potential improvement could be assessed by simple comparison with a single floodability index. Besides, the exploration of combinations of topography and SAR methods could be quite valuable. Indeed, as previously explained, the topography method can be extended at the global scale quite easily since topographic indices are available. On the other hand, the SAR method

is based on observations and has the great advantage of capturing flood dynamics independent to topography (i.e., anthropogenic structures or irrigation). For instance, linear combinations of SAR-derived and topography-based floodability indices could be envisaged, potentially with different weights depending on the environment (there are some techniques to optimally weight two sources of information on a same parameter, this is used for instance in the ESA WACMOS soil moisture dataset to mix the passive and active microwave retrieval of soil moisture). Also, water maps from SAR observations could be included into the Neural Network training of the topography -based floodability index, as well as other indicators to better account for isolated small water bodies or the type of environment (e.g., land use, land cover, soil characteristics, etc.).

Finally, the application of the SAR method should be explored over different hydro-climatic regions (e.g., Amazon, Niger, Mekong). The impact of the presence or not of extreme events in the SAR sampling is also a way of potential improvements. To demonstrate the value of the merged GIEMS-SAR product for hydrological studies, it is proposed to analyse in more details the time series over different test cases. In particular, seasonal cycles, trends and interannual variability could be extracted at the local and regional scales. To assess the hydrological consistency of the merged product, results could be compared to other datasets, such as other inundation estimates (e.g. from LandCover_cci or MODIS), soil moisture (e.g. from SoilMoisture_cci or the WACMOS project), in situ water level or discharge data or terrestrial water storage from the GRACE spatial gravimetry mission (for basin scale water mass variability).

The present work helped us to better understand the potential of such downscaling approaches, their advantages and drawbacks, and all of the potential improvements make them a very promising way to develop a long time series (several decades) of high resolution inundation maps by combining all the available information (including IR/VIS imagery, SAR, low-resolution passive/active microwave, topography, etc.).

6.3 Potential applications

As stated previously, the merged GIEMS-SAR product will be highly valuable for climate studies as well as for analyses of anthropogenic impacts. Following similar methodologies as those developed by Munier et al. (2012) on the relationship between the global and regional runoff and climate variability, statistical and frequential comparisons between the surface water extent variability and a panel of climate indices related to the main large scale phenomena (such as ENSO or the Atlantic Multidecadal Oscillation) could be performed. As for most parts of the world, the hydro-climatic conditions are strongly related to such phenomena, it is expected that surface water extent shows similar relationships, even though such a result is still not clearly identified for the smallest water bodies. This would provide a necessary first step to quantify the contribution of small water bodies to the climate variability, as well as feedback effects.

In addition, the potential link between surface water extent and anthropogenic factors and population pressure (e.g. land use change, agriculture, urbanisation) could be explored. Such analysis could follow the study by Prigent et al. (2012) that related an overall decline in global average maximum inundated area to large increases in population over the last two decades, suggesting a global scale effect of human activities on continental surface freshwater. The high-resolution merged product should partly confirm these results if applied on test cases that are either highly impacted by anthropogenic factors (e.g. Mekong or Mississippi basins) or driven by natural conditions (e.g. Amazon or Congo basins). As it could be done with climate indices, the comparison with different

indices related to human activities could be performed, such as population growth, water management strategies or land use changes. The high-resolution inundation estimates could also be used to compute water volume changes (Frappart et al., 2012) and river discharge estimates; the impact of spatial resolution (from GIEMS to merge GIEMS-SAR) could be assessed, which should provide significant analyses of the potential benefits that could be expected from Sentinel-1 data.

7 Publication

Munier, S., F. Aires and C. Prigent (2016). GIEMS-SAR: a high resolution monthly dataset to study surface water extent dynamics – application on the Danube Basin, J. of Hydrometeorology, in preparation.

8 References

Aires, F., F. Papa and C. Prigent (2013). A long-term, high-resolution wetland dataset over the Amazon basin, downscaled from a multi-wavelength retrieval using SAR, J. of Hydrometeorology, 14, 594-6007.

Aires, F., Papa, F., Prigent, C., Crétaux, J. F., & Berge-Nguyen, M. (2014). Characterization and Space–Time Downscaling of the Inundation Extent over the Inner Niger Delta Using GIEMS and MODIS Data. Journal of Hydrometeorology, 15(1), 171-192.

Downing, J. A., Prairie, Y. T., Cole, J. J., Duarte, C. M., Tranvik, L. J., Striegl, R. G., ... & Middelburg, J. J. (2006). The global abundance and size distribution of lakes, ponds, and impoundments. Limnology and Oceanography, 51(5), 2388-2397.

Fluet-Chouinard E., Lehner B., Rebelo L.M., Papa F., Hamilton S.K. (2015): Development of a global inundation map at high spatial resolution from topographic downscaling of coarse-scale remote sensing data. Remote Sensing of Environment 158: 348-361. dx.doi.org/10.1016/j.rse.2014.10.015

Hess, L. L., Melack, J. M., Novo, E. M., Barbosa, C. C., & Gastil, M. (2003). Dual-season mapping of wetland inundation and vegetation for the central Amazon basin. Remote Sensing of Environment, 87(4), 404-428.

Kuenzer, C., Guo, H., Huth, J., Leinenkugel, P., Li, X., & Dech, S. (2013a). Flood mapping and flood dynamics of the Mekong delta: Envisat-ASAR-WSM based time series analyses. Remote Sensing, 5(2), 687-715.

Kuenzer, C., Guo, H., Schlegel, I., Tuan, V. Q., Li, X., & Dech, S. (2013b). Varying scale and capability of envisat ASAR-WSM, TerraSAR-X Scansar and TerraSAR-X Stripmap data to assess urban flood situations: A case study of the Mekong delta in Can Tho province. Remote Sensing, 5(10), 5122-5142.

Lehner, B., and Döll, P. (2004). Development and validation of a global database of lakes, reservoirs and wetlands. Journal of Hydrology, 296(1), 1-22.

Lehner, B., Verdin, K., & Jarvis, A. (2006). HydroSHEDS technical documentation, version 1.0. World Wildlife Fund US, Washington, DC, 1-27.

Lewis, A. J., and Henderson, F. M. (1998). Geomorphic and hydrologic applications of active microwave remote sensing. Principles and applications of imaging radar. Manual of Remote Sensing, 567-629.

Miolane, L., Aires, P., Prigent, C., Fluet-Chouinard, E. And Lehner, B. (2016). Global, high spatial-resolution, dynamic and long-term inundation extent dataset, downscaled from GIEMS using topography information. Submitted to Journal of Hydrometeorology.

Munier, S., Palanisamy, H., Masongrande, P., Cazenave, A. and Wood, E.F. (2012). Global runoff anomalies over 1993-2009 estimated from coupled Land-Ocean-Atmosphere water budgets and its relation with climate variability. Hydrology and Earth System Sciences, 16, 3647-3658. doi:10.5194/hess-16-3647-2012.

Nakaegawa, T. (2012). Comparison of water-related land cover types in six 1-km global land cover datasets. Journal of Hydrometeorology, URL http://journals.ametsoc.org/doi/abs/10.1175/JHM-D-10-05036.1.

Parente, C. (2013). TOA reflectance and NDVI calculation for Landsat 7 ETM+ images of Sicily. In Proceedings in EIIC-The 2nd Electronic International Interdisciplinary Conference (No. 1).

Papa, F., Prigent, C., Aires, F., Jimenez, C., Rossow, W. B., & Matthews, E. (2010). Interannual variability of surface water extent at the global scale, 1993–2004. Journal of Geophysical Research: Atmospheres (1984–2012), 115(D12).

Prigent, C., Matthews, E., Aires, F., & Rossow, W. B. (2001). Remote sensing of global wetland dynamics with multiple satellite data sets. Geophysical Research Letters, 28(24), 4631-4634.

Prigent, C., Papa, F., Aires, F., Rossow, W. B., & Matthews, E. (2007). Global inundation dynamics inferred from multiple satellite observations, 1993–2000. Journal of Geophysical Research: Atmospheres (1984–2012), 112(D12).

Prigent, C., Papa, F., Aires, F., Jimenez, C., Rossow, W. B., & Matthews, E. (2012). Changes in land surface water dynamics since the 1990s and relation to population pressure. Geophysical Research Letters, 39(8).

Rosenqvist, A., Shimada, M., Chapman, B., Freeman, A., De Grandi, G., Saatchi, S., & Rauste, Y. (2000). The global rain forest mapping project-a review. International Journal of Remote Sensing, 21(6-7), 1375-1387.

Zhu, Z. and Woodcock, C. E., Object-based cloud and cloud shadow detection in Landsat imagery, Remote Sensing of Environment (2012), doi:10.1016/j.rse.2011.10.028